ACS APPLIED MATERIALS & INTERFACES

Research Article

www.acsami.org

A Bifunctional Copolymer Additive to Utilize Photoenergy Transfer and To Improve Hole Mobility for Organic Ternary Bulk-Heterojunction Solar Cell

Cheng-Yu Chi, Ming-Chung Chen, Der-Jang Liaw, Han-Yu Wu, Ying-Chi Huang, and Yian Tai*

Department of Chemical Engineering, National Taiwan University of Science and Technology, Taipei 10617, Taiwan

Supporting Information

ABSTRACT: To realize the high efficiency organic photovoltaics (OPVs), two critical requirements have to be fulfilled: (1) increasing the photon energy absorption range of the active layer, and (2) improving charge separation and transport in the active layer. This study reports the utilization of THC8, a novel fluorescence-based polymer containing propeller-shaped di-triarylamine and fluorene moieties in the active layer consisting of poly-3-hexylthiophene and [6,6]-phenyl-C61-butyric acid methyl ester to form a ternary bulk heterojunction. The results showed that the high absorbance and strong fluorescence of THC8 at 420 and 510 nm, respectively, broadened the spectral absorption of the OPV, possibly through Förster resonance energy transfer. In addition, the morphology of the device active layer was improved with the addition of a suitable amount of THC8. Consequently, the charge transport property of the active layer was improved. The best power conversion efficiency (PCE) of the device with THC8 was 3.88%, a 25% increase compared to the PCE of a pristine OPV.

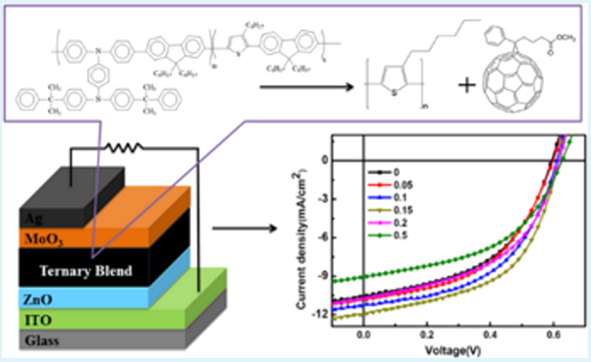

KEYWORDS: *organic solar cell, Förster resonance energy transfer, hole mobility, ternary bulk heterojunction*

INTRODUCTION

Over the past decade, organic photovoltaics (OPVs) have attracted significant attention for the production of solar energy owing to their potential advantages, such as low cost, flexibility, lightweight, large area, and simple processability.[1,2] Typically, an OPV employs only two organic semiconductors with distinctive electrical properties. One is a donor (p-type), and the other is an acceptor (n-type). These two materials form p−n junctions in the active layer.[3] Upon light irradiation, the acceptor and/or donor absorbs light, resulting in the formation of a stable excited state called the exciton. As the photogenerated exciton has large binding energy, the driving force offered by the p−n junction is required for the dissociation of excitons to free carriers.[4] Then, the carriers, which are transported through the active layer, are collected by the cathode and anode.

Among the various OPVs, bulk-heterojunction (BHJ) solar cells have proven to be the most efficient configuration for the dissociation of excitons. In a BHJ OPV, a p-type material (e.g., conjugated polymer) and an n-type material (e.g., fullerene derivative) are mixed to form the active layer.[5,6] This mixed configuration increases the number of p−n junctions, which, in turn, improves the exciton dissociation efficiency. Recently, the research efforts have led toward the achievement of the power conversion efficiency (PCE) to 9.2% for BHJ devices[7] and even up to over 10% with a tandem structure.[8]

In the BHJ system, poly(3-hexylthiophene) (P3HT) and [6,6]-phenyl-C61-butyric acid methyl ester (PCBM) are the most commonly used p- and n-type materials, respectively.[9,10] However, P3HT, with a band gap of ∼2 eV, absorbs approximately only 20% of the incident light, thereby limiting the maximum available photocurrent density.[11] Recently, a promising approach was developed for improving light harvesting by designing and synthesizing low band gap polymers that absorb a broad spectrum of light.[12] However, the syntheses of low band gap polymers are complex and expensive. An alternative method is to construct a tandem cell, which couples two donors having different band gaps.[13,14] Though this led to the wider range absorption of the solar spectrum of the OPV, the fabrication of a tandem cell is a challenging task. The major issue is the obligation of a suitable interlayer, which satisfies the requirements of good electrical connection between two subcells, is optically transparent, and is robust enough to protect the bottom cell from being damaged by the solution process of the top cell. In addition, coupling of appropriate absorbers to maximize solar spectrum absorption and controlling the thickness of each layer to optimize the optical and electrical properties of the device also complicate the fabrication of tandem OPVs. Another drawback of the

Received: February 27, 2014
Accepted: July 9, 2014
Published: July 17, 2014

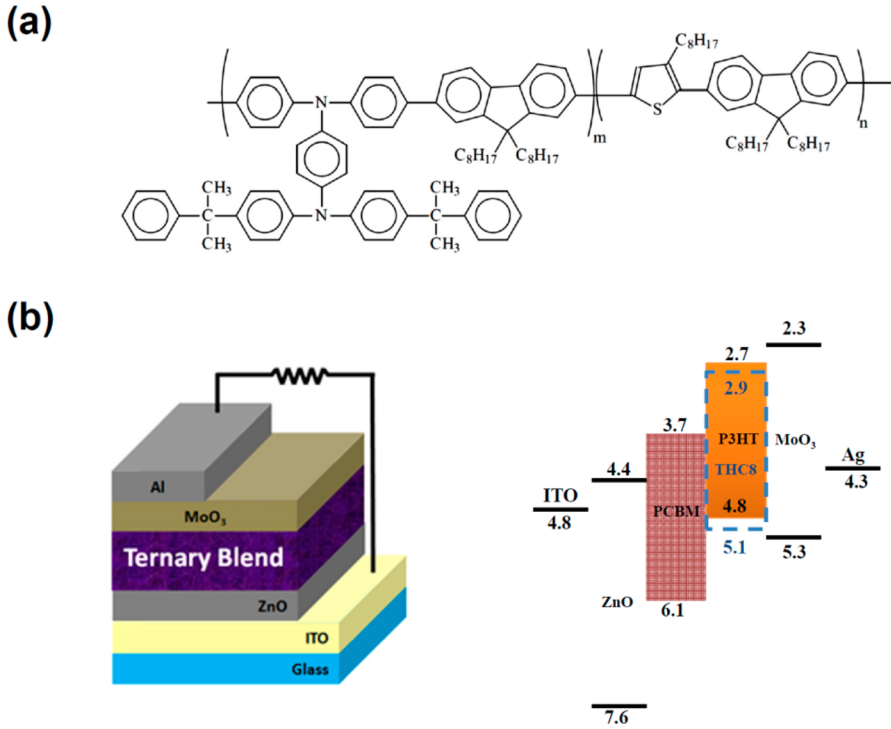

Figure 1. Chemical structure of THC8 (a), and the structure and the energy alignment of the OPV device (b).

P3HT/PCBM system is the unbalanced charge transport.[15,16] The hole mobility of P3HT is on the order of 10^{-4} m^2 V^{-1} S^{-1}, whereas the electron mobility of PCBM is 1 order of magnitude higher. Such mismatch results in charge transport imbalance due to the faster movement of electrons toward the cathode compared to the movement of holes toward the anode. As a consequence, electrons accumulate at the interface of the PCBM/cathode, causing enhanced charge recombination, which severely affects the efficiency of the device.

Recently, a sophisticated approach using ternary solar cells has been developed to improve the efficiency of BHJ OPVs.[17] In a ternary solar cell, a third component is mixed in the host BHJ active layer to improve the efficiency of the OPV device through one of the following two mechanisms.[18−20] The first mechanism is the increase in energy transfer. For instance, an absorber that absorbs alternative wavelengths to the original active layer can be added to the BHJ to increase the efficiency of sunlight harvest. These absorbers can either generate excitons or improve long-range exciton migration through Förster-type resonance energy transfer (FRET).[21,22] The second mechanism involves enhancing the charge transfer. For example, a third component can be added to optimize the morphology of the polymer chain,[19] to adjust the phase separation of the p- and n- components,[20,23] to form a cascade structure,[24] or to improve the hole mobility of the active layer.[25]

Several studies have reported improvements in OPV efficiency using FRET with small organic dye molecules.[22,26,27] However, such a process might suffer from low lifetime because the small dye molecules are environmentally sensitive, when compared to polymers.[28] To our best knowledge, there are no reports on utilizing FRET in OPVs with a polymer as the third component. Among all the ternary approaches that have been explored for improving OPV efficiency, in most cases, the third component has only one function that either increases the light harvest or enhances the charge transfer.

In this study, we demonstrated the concept by synthesizing and utilizing a dual-functional copolymer (THC8) to improve the hole mobility and to simultaneously employ FRET for a ternary BHJ OPV, which consisted of P3HT and PCBM as the active layer. The di-triarylamine-fluorene-based copolymer has two components: the di-triarylamine-fluorene structure that was proven to be effective in enhancing the hole mobility of the active layer,[24] while the thiophene-fluorene component might act as the FRET donor.[29] Owing to the unique structure of THC8, both energy transfer and charge transfer of the active layer could be improved, increasing the overall efficiency of OPVs. In addition, the 2,2-diphenyl propane structure in THC8 could enhance the thermal stability and chemical resistance of the polymer chain,[25] which, in principle, could extend the lifetime of the efficiency improvement on the ternary OPV in comparison with small organic molecular additives.

EXPERIMENTAL SECTION

The synthesis process of THC8 is described in the Supporting Information. The M_n, M_w, and PDI of THC8 were 2.9×10^4, 4.2×10^4, and 1.43, respectively. To fabricate the OPV device, ITO (the sheet resistance of 15 Ω/□) substrates were acquired from Merck. The P3HT was purchased from Rieke Metals (#BS19-04), PCBM was purchased from Solenn, and zinc acetate (ZnAc) was used as received from the Sigma-Aldrich. The 70 nm thick ZnO was first fabricated on the cleaned ITO/glass substrate with the reported method.[30,31] The P3HT, PCBM, and THC8 were blended together in the ratio of 1:0.6:X (X = 0, 0.05, 0.1, 0.15, 0.2, and 0.5) by weight, respectively. The corresponding weight ratios (wt %) of THC8 to the total weight were 0, 3, 6, 9, 11, and 24 wt %, respectively. The blends were stirred at 45 °C for 14 h in nitrogen ambient. Afterward, the ∼150 nm active layers were spin-casted on ZnO thin film, followed by sequentially solvent annealing and thermal annealing. After that, 10 nm MoO_3 and

100 nm silver were thermally deposited on top of the active layer consecutively. The active area of the device was 0.04 cm^2.

To fabricate the hole-only device, a P3HT:PCBM:THC8 blend was spin-coated on a PEDOT:PSS/ITO substrate, followed by the deposition of 20 nm MoO_3 on top of the blend layer. Finally, 60 nm thick Au was thermal evaporated on top of the MoO_3 as the electrode.

Cyclic voltammetry (CV) was performed with a CHI model 660C potentiostat. *J*–*V* characteristics of the devices were obtained via a Keithley 2400 multimeter under dark and illumination conditions of a 100 mW/cm^{-2}, AM 1.5G, and 1 sun solar simulator (Newport-Oriel 500 W) that was calibrated by a reference silicon (Si) cell prior to the measurements. The *J*–*V* characteristics demonstrated average results of 20 devices, and the error bars were presented in the data table. The external quantum efficiency (EQE) was measured using a 300 W Xe lamp-based solar simulator (Oriel arc lamp #66160) with a calibrated Si photodiode. The optical properties of the active layers and the devices were investigated using UV–vis spectroscopy (Jasco-V-670) and photoluminescence (PL) spectroscopy (Dong Woo Option, PDL 800-B). All the spectra were normalized with respect to the actual film thicknesses. The surface roughness and morphology of the devices were probed by atomic force microscopy (AFM; Digital Nanoscope IIIA) using the tapping mode.

RESULTS AND DISCUSSION

The chemical structure of THC8 is shown in Figure 1a. The highest occupied molecular orbital (HOMO) and the lowest unoccupied molecular orbital (LUMO) of THC8, determined by cyclic voltammetry (CV) measurements, were 5.1 and 2.9 eV, respectively. From the energy diagram aspect (Figure 1b), it is clear that THC8 is suitable to be added in the P3HT:PCBM active layer to form a ternary OPV.

To behave as a FRET donor, there are three requirements that must be fulfilled: (1) it must be a strong fluorophore, (2) there must be a large overlap between the fluorescence spectrum of the FRET donor and the absorbance spectrum of the acceptor, and (3) the donor and the acceptor (THC8 and P3HT, respectively) must be within one Förster radius (several nm) from each other. The UV–vis spectra of pure THC8 and P3HT, and the photoluminescence (PL) spectrum of THC8, are shown in the inset of Figure 2. It is clear that THC8 absorbs UV light centered at ~410 nm and re-emits the strong fluorescence at ~510 nm. The fluorescence of THC8 is well within the absorption region of P3HT (400–650 nm).

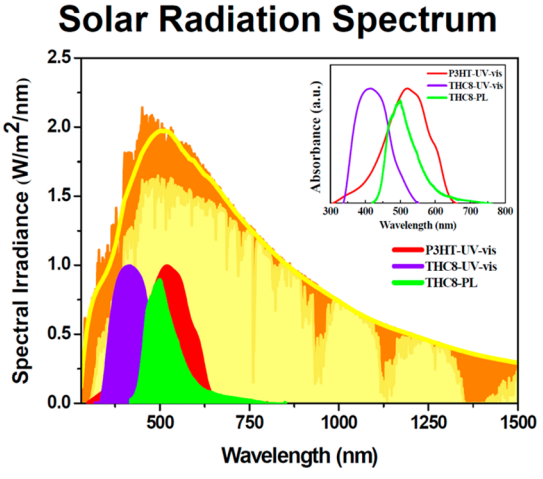

Figure 2. Absorption and PL spectra of THC8, the absorption spectrum of P3HT (inset), and their superposition on the solar spectrum.

Figure 2 shows the superposition of the above three spectra with a solar spectrum. It can be seen that THC8 is a good FRET donor in a P3HT-based OPV, as it fluoresces strongly and can absorb light energy from the UV region and transfer it to P3HT for enhanced light harvesting by P3HT.[32] From the overlap between the PL spectrum of THC8 and the absorption of P3HT, we calculated the Förster radius to be ~4.8 nm (Supporting Information), which concluded that possibly FRET occurred between THC8 and P3HT.

To further confirm that THC8 is a good FRET donor, we investigated the PL spectra of pure THC8, P3HT, and the mixture of THC8/P3HT with different P3HT contents in chlorobenzene. The spectra obtained on exciting at 370 nm are shown in Figure 3. The emission maxima of pristine THC8 and

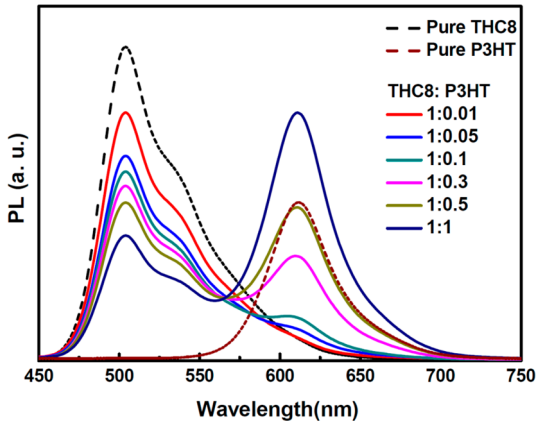

Figure 3. PL spectra of pure THC8, P3HT, and the mixture of THC8/P3HT having different P3HT concentrations in chlorobenzene.

P3HT were centered at ~505 and ~610 nm, respectively. With increasing P3HT content, the emission of THC8 decreased with a simultaneous increase in the emission of P3HT. At a 1:1 ratio of THC8:P3HT, the emission of THC8 declined significantly and a noticeable P3HT emission was observed. The intensity of the P3HT emission at a 1:1 ratio was even higher than that of the pure P3HT. Since the emission of pure P3HT at the excitation of 375 nm is not strong due to the low absorption cross section, the markedly high PL of THC8:P3HT (1:1 ratio) suggested the energy transfer from THC8 through FRET.[33,34] In addition, we performed PL measurements on THC8 thin films with different amounts of added P3HT. The preparation method (solvent, spin-coating parameters, annealing process) of the films is identical to the method followed during the preparation of the films in actual solar cell device. Similar results that the addition of P3HT caused a decrease in the PL of THC8 and an increase in the PL of P3HT can also be observed (Figure S1 in the Supporting Information).

The *J*–*V* curves of the devices having different THC8 concentrations under light irradiation (AM 1.5G, 1 sun) are demonstrated in Figure 4, and the corresponding device operating parameters are shown in Table 1. The PCE (%) of the cell devices with various contents of THC8 in P3HT/PCBM (1:0.6) are 3.10 (0), 3.15 (0.05), 3.52 (0.1), 3.88 (0.15), 3.23 (0.2), and 2.74 (0.5). Apparently, the PCE increases with increasing THC8 concentration from 0 up to 0.15. The highest J_{sc} value of 11.92 mA/cm^2, FF of 52.54%, and PCE of 3.88% could be achieved. The respective values in the pristine device were 10.55 mA/cm^2, 48.31%, and 3.10%. The increase in PCE

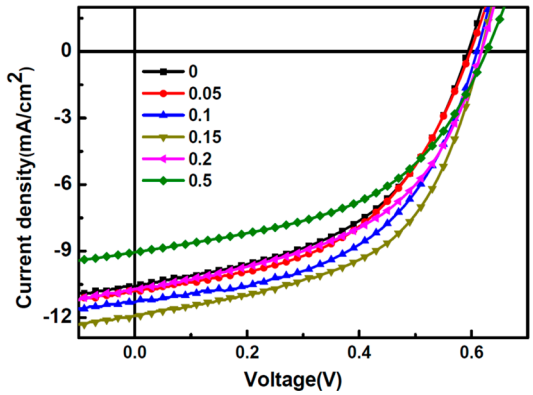

Figure 4. *J*−*V* curves of the OPV devices under light irradiation having different THC8 concentrations.

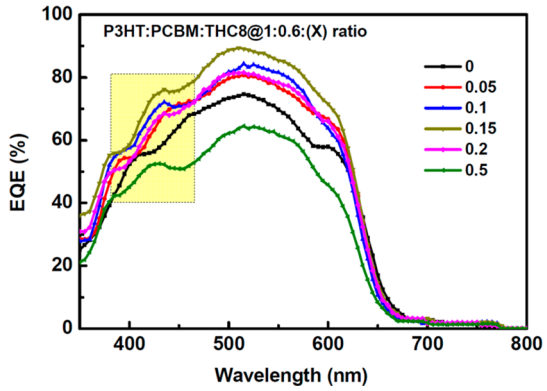

Figure 5. External quantum efficiency (EQE) measurements on the OPV devices with different THC8 concentrations.

from 3.10% to 3.88% corresponds to a 25% increase in the overall PCE. On increasing the concentration of THC8 to 0.2, the performance of the OPV device decreased, although the PCE of the 0.2 device was still greater than that of the pristine OPV. However, a significant decrease of the device performance was observed upon the addition of 0.5 THC8. The J_{sc} dropped to 9.05 mA/cm^2, resulting in a severely decreased PCE of 2.74%, indicating the appreciable effects of THC8 on the active material matrix at higher mixing content.

The V_{oc} values of the OPV devices were maintained in the range of 0.61−0.63 V, indicating that the properties of the donor (HOMO) and the acceptor (LUMO) were dominated by P3HT and PCBM, respectively, regardless of the amount of THC8 added to the active layer. The improvement in J_{sc} values could be attributed to the following reasons: (1) improved charge mobilities of the active layer facilitated by THC8,[24] (2) increased charge generation as THC8 might act as an active photon-absorbing material that generated charges,[17] and (3) the increasing photon energy absorption through FRET of THC8 to P3HT.[35]

To confirm the effects of THC8 on the improvement in J_{sc}, we performed external quantum efficiency (EQE) measurements on the OPV devices having different THC8 concentrations. In other literatures, the EQE of the ternary OPV system has shown either a local enhancement that corresponds to the absorption of the third component[36,37] or an overall enhancement through the entire spectral range.[20,24] However, the EQE results in Figure 5 show the enhancements both over the entire spectra and also in the local region for the devices with TCH8 contents up to 0.2, in comparison with the pristine device. For the TCH8 contents up to 0.2, we observed a significant enhancement in EQE over the entire spectral range (375−700 nm), whereas EQE decreased significantly for the 0.5 device, which was fairly consistent with the PCE results. On the other hand, a notably new peak was observed in the EQE spectra (highlighted area) between 400 and 470 nm in all the devices with THC8. This peak could have resulted from THC8 as the absorption maximum of THC8 was within this range. Although the absorption of PCBM is also in this range,[38] still, we believe that the major contribution to the EQE at this range was due to the THC8 for the following reason: The contents of the PCBM were indeed decreased with the increase of the amount of THC8. For example, comparing to the pristine device, the THC8 was increased from 0 to 24% (in total weight) at a higher ratio (THC8 = 0.5) while the PCBM weight % was decreased from 37.5% to 28.6%. As the excess THC8 should decline the phase separation and the crystallinity of PCBM in the active layer[20] and since the content of PCBM was decreased with the increase of content of THC8, the contribution of PCBM to EQE at a higher THC8 ratio should be decreased; at least the contribution of PCBM should not affect evidently the increase in the region of ∼420 nm. However, compared to the EQE of the pristine device, a clear peak appeared at ∼420 nm for all devices with THC8 even for the high contents (0.5) film. (Figure 5, highlighted part). Therefore, we believe that THC8 contributed primarily to the increase of EQE in the region of ∼420 nm; although the effect of the PCBM cannot completely be ruled out.

To exclude the effect due to the photocharge generation by THC8/PCBM that most-probably developed the new peak in EQE in the region of ∼420 nm, we fabricated an OPV device by utilizing a THC8 and PCBM blend (1:1) as the active layer and performed UV−vis absorption and EQE measurements. The inset in Figure S2 (Supporting Information) shows considerable absorption between 300 and 450 nm of the THC8:PCBM layer. However, no EQE was observed in that range, as shown in Figure S2, which indicated the absence of photocharge generation between THC8/PCBM. Therefore, the assumption that THC8 could be an active material is ruled out. As a result, we suggested that the newly generated peak at ∼420

Table 1. Device Characteristics of the OPV Having Different THC8 Concentrations

THC8 ratio	J_{sc} (mA/cm^2)	V_{oc} (V)	efficiency η(%)	FF (%)
0	10.55 ± 0.33	0.60 ± 0.01	3.10 ± 0.14	48.31 ± 0.92
0.05	10.79 ± 0.26	0.60 ± 0.01	3.15 ± 0.12	48.68 ± 0.53
0.1	11.27 ± 0.21	0.62 ± 0.02	3.52 ± 0.06	50.34 ± 0.40
0.15	11.92 ± 0.29	0.62 ± 0.01	3.88 ± 0.07	52.54 ± 0.16
0.2	10.73 ± 0.16	0.62 ± 0.01	3.23 ± 0.15	48.58 ± 0.23
0.5	9.05 ± 0.47	0.63 ± 0.01	2.74 ± 0.08	48.03 ± 0.52

nm in EQE was due to photon energy transfer from THC8 to P3HT.

On the other hand, the enhancement in EQE over the entire spectral range could not be explained by FRET, as THC8 does not absorb at wavelengths higher than 520 nm. To investigate the effect of THC8 on the improvement of the entire EQE range, we investigated the electrical properties of the devices having different THC8 concentrations by fabricating the hole-only devices and measuring the hole mobilities.[39−41] The hole mobility (μ_h) is determined by precisely fitting the plot of the dark current versus the $J-V$ curve of the single carrier devices with the SCLC model. When sufficient voltage is applied to this hole-only device, the transport of holes through the polymer film is limited by the accumulated space charge. The SCLC is described by the Mott−Gurney equation

$$J = \frac{9}{8}\varepsilon_r\varepsilon_0\mu_h\frac{V^2}{L^3} \quad (1)$$

where ε_0 is the permittivity of free space, ε_r is the dielectric constant of the polymer, μ_h is the hole mobility, V is the voltage drop across the device, and L is the active layer thickness of the film. The applied voltage has been corrected for the built-in voltage (V_{bi}), which arises from the difference in the work function of the contacts, so that $V = V_{applied} - V_{bi}$. V_{bi} values are 0.1 V for hole-only devices. The slope of the $J^{0.5}-V$ curves shown in Figure 6 presents the relative hole mobilities of the

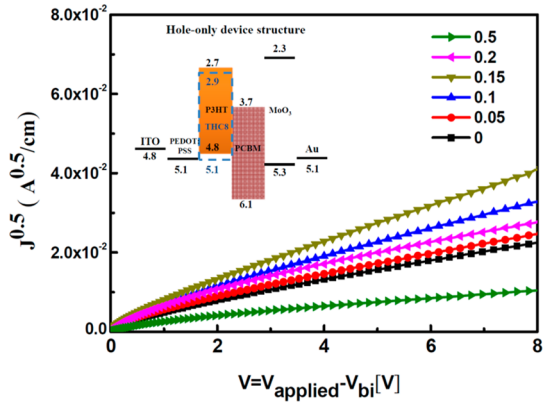

Figure 6. $J^{0.5}-V$ curves of the "hole-only" device having different THC8 concentrations.

active layers with different THC8 concentrations.[39,19,42] The slope increased from 0 of THC8 up to 0.2 with the highest value at 0.15, which declined drastically upon further addition of TCH8 to 0.5. The improved hole mobilities were also reflected in the fill factor (FF %), as shown in Table 1. An enhancement in FF values from 48.31% to 52.54% upon the addition of 0.15 of THC8 suggested a reduction in charge recombination in the active layer due to improved hole mobility. Thus, we concluded that the hole mobilities of the active layer increased with the addition of THC8 up to 0.2, leading to improved EQE over the entire spectrum range. This improvement was possibly due to the reason that the morphology of the active layer and the phase separation between P3HT and PCBM changed upon the addition of a suitable amount of THC8, which led to the formation of appropriate pathways for the carrier transport.[20] As a result, the hole mobilities increased. However, when the excess amount of THC8 was added in the active layer, the marked decrease in OPV performance can be observed. This can be explained by the vast decrease in the order of P3HT and abolition of the optimized phase separation in the active layer.[20] Although the polymer chains of P3HT stacked well during the solvent annealing process, its order could be destroyed if it was blended with large quantities of THC8. This was confirmed by XRD results, shown in Figure S3 (Supporting Information), which reveal that unfavorable morphological changes occur that deteriorate charge separation and transport. As a consequence, the devices with higher concentrations of THC8 exhibited relatively low current densities and PCE.

To further confirm our assumption, physical changes in the morphology of P3HT:PCBM (1:0.6) films at various THC8 concentrations were investigated by tapping-mode atomic force microscopy (AFM) (Figure 7). The images demonstrated a

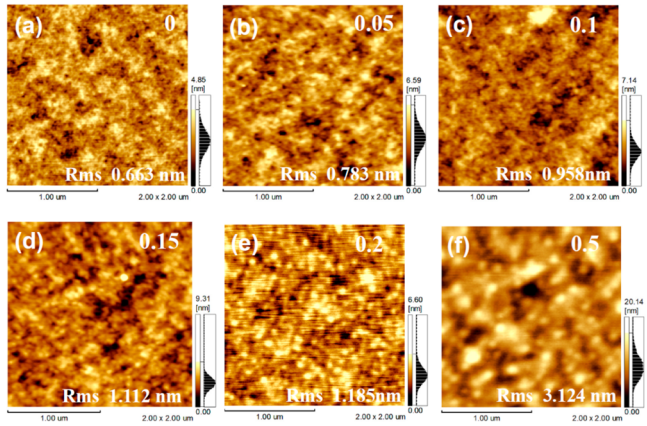

Figure 7. Atomic force microscope morphological images of the P3HT:PCBM (1:0.6) films incorporating various amounts of THC8.

smooth film morphology for the blends with THC8 concentration ranging from 0% to 0.2%; the constitutions were fairly uniform with mild phase separation between the polymers and PCBM (Figure 7a−e). Such constitutions are most likely corresponding to smaller carrier donor and acceptor phases that increase the possibility for excitons reaching D−A interfaces and being dissociated. Although THC8 is an amorphous polymer, it could mix well with P3HT due to $\pi-\pi$ interaction and the thiophene units in the polymer chain.[43] With a moderate amount of THC8, the crystallinity of the P3HT in the active layer blend can still be kept intact.[44,45] However, with increasing THC8 content to 0.5, surface roughness increased significantly (Figure 7f), probably caused by the spreading of aggregations of THC8 and P3HT mixing over the entire film due to the addition of an excess amount of the THC8,[18,20] which resulted in the deterioration of the optimized phase separation of P3HT and PCBM, which caused the poor charge separation, transport, and severe electron and hole recombination. As a consequence, the OPV having higher concentrations of THC8 exhibited lower values of J_{sc}, FF, and the overall PCE.

CONCLUSION

In conclusion, we demonstrated the concept of improving the efficiency of an OPV by utilizing THC8, a bifunctional polymer that enhances charge transport and possibly broadens the spectral absorption through FRET. The J_{sc} improved from 10.55 to 11.97 mA/cm^2 and the FF increased from 48.31 to 52.54% with the addition of 0.15 of THC8, thereby improving

the efficiency from 3.10 to 3.88%. This concept paves the way for a new paradigm toward improving the OPV performance and might be utilized in other low band gap polymer single junction devices to reach PCE values higher than 10% in the future.

■ ASSOCIATED CONTENT

Supporting Information

Synthesis process and the solubility of THC8; detailed calculation of the Förster radius; PL spectra of thin films of pure THC8, P3HT, and the mixed THC8/P3HT featuring different P3HT contents; EQE spectrum of the device with THC8:PCBM (1:1) as active layer; and XRD results of the P3HT:PCBM thin films featuring different THC8 contents. This material is available free of charge via the Internet at http://pubs.acs.org.

■ AUTHOR INFORMATION

Corresponding Author

*Phone: +886-2-2737-6620. Fax: +886-2-2737-6644. E-mail: ytai@mail.ntust.edu.tw.

Notes

The authors declare no competing financial interest.

■ ACKNOWLEDGMENTS

The authors are grateful to the Center for Condensed Matter Sciences of NTU for the technical support. This project was funded by the Academia Sinica and the Ministry of Science and Technology.

■ REFERENCES

(1) Ma, S.; Fu, Y.; Ni, D.; Mao, J.; Xie, Z.; Tu, G. Spiro-fluorene Based 3D Donor towards Efficient Organic Photovoltaics. *Chem. Commun.* **2012**, *48*, 11847−11849.

(2) O'Carroll, D. M.; Petoukhoff, C. E.; Kohl, J.; Yu, B.; Carter, C. M.; Goodman, S. Conjugated Polymer-Based Photonic Nanostructures. *Polym. Chem.* **2013**, *4*, 5181−5196.

(3) Anthony, J. E.; Facchetti, A.; Heeney, M.; Marder, S. R.; Zhan, X. N-Type Organic Semiconductors in Organic Electronics. *Adv. Mater.* **2010**, *22*, 3876−3892.

(4) Koster, L. J. A.; Mihailetchi, V. D.; Ramaker, R.; Xie, H.; Blom, P. W. M. In Light Intensity Dependence of Open-Circuit Voltage and Short-Circuit Current of Polymer/Fullerene Solar Cells. *Proc. SPIE - Int. Soc. Opt. Eng.* **2006**, *6192*, 61922G.

(5) Servaites, J. D.; Yeganeh, S.; Marks, T. J.; Ratner, M. A. Efficiency Enhancement in Organic Photovoltaic Cells: Consequences of Optimizing Series Resistance. *Adv. Funct. Mater.* **2010**, *20*, 97−104.

(6) Treat, N. D.; Brady, M. A.; Smith, G.; Toney, M. F.; Kramer, E. J.; Hawker, C. J.; Chabinyc, M. L. Interdiffusion of PCBM and P3HT Reveals Miscibility in a Photovoltaically Active Blend. *Adv. Energy Mater.* **2011**, *1*, 82−89.

(7) He, Z.; Zhong, C.; Su, S.; Xu, M.; Wu, H.; Cao, Y. Enhanced Power-Conversion Efficiency in Polymer Solar Cells Using an Inverted Device Structure. *Nat. Photonics* **2012**, *6*, 591−595.

(8) You, J.; Chen, C. C.; Hong, Z.; Yoshimura, K.; Ohya, K.; Xu, R.; Ye, S.; Gao, J.; Li, G.; Yang, Y. 10.2% Power Conversion Efficiency Polymer Tandem Solar Cells Consisting of Two Identical Sub-cells. *Adv. Mater.* **2013**, *25*, 3973−3978.

(9) Labram, J. G.; Kirkpatrick, J.; Bradley, D. D. C.; Anthopoulos, T. D. Impact of Fullerene Molecular Weight on P3HT:PCBM Microstructure Studied Using Organic Thin-Film Transistors. *Adv. Energy Mater.* **2011**, *1*, 1176−1183.

(10) Meyer, M. W.; Larson, K. L.; Mahadevapuram, R. C.; Lesoine, M. D.; Carr, J. A.; Chaudhary, S.; Smith, E. A. Scanning Angle Raman Spectroscopy of Poly(3-hexylthiophene)-Based Films on Indium Tin Oxide, Gold, and Sapphire Surfaces. *ACS Appl. Mater. Interfaces* **2013**, *5*, 8686−8693.

(11) Forrest, S. R.; Thompson, M. E. Introduction: Organic Electronics and Optoelectronics. *Chem. Rev.* **2007**, *107*, 923−925.

(12) Yue, W.; Huang, X.; Yuan, J.; Ma, W.; Krebs, F. C.; Yu, D. A Novel Benzodipyrrolidone-Based Low Band Gap Polymer for Organic Solar Cells. *J. Mater. Chem. A* **2013**, *1*, 10116−10119.

(13) Gevaerts, V. S.; Furlan, A.; Wienk, M. M.; Turbiez, M.; Janssen, R. A. J. Solution Processed Polymer Tandem Solar Cell Using Efficient Small and Wide Bandgap Polymer: Fullerene Blends. *Adv. Mater.* **2012**, *24*, 2130−2134.

(14) Li, K.; Li, Z.; Feng, K.; Xu, X.; Wang, L.; Peng, Q. Development of Large Band-Gap Conjugated Copolymers for Efficient Regular Single and Tandem Organic Solar Cells. *J. Am. Chem. Soc.* **2013**, *135*, 13549−13557.

(15) Faist, M. A.; Shoaee, S.; Tuladhar, S.; Dibb, G. F. A.; Foster, S.; Gong, W.; Kirchartz, T.; Bradley, D. D. C.; Durrant, J. R.; Nelson, J. Understanding the Reduced Efficiencies of Organic Solar Cells Employing Fullerene Multiadducts as Acceptors. *Adv. Energy Mater.* **2013**, *3*, 744−752.

(16) Huang, B.; Glynos, E.; Frieberg, B.; Yang, H.; Green, P. F. Effect of Thickness-Dependent Microstructure on the Out-of-Plane Hole Mobility in Poly(3-hexylthiophene) Films. *ACS Appl. Mater. Interfaces* **2012**, *4*, 5204−5210.

(17) Lobez, J. M.; Andrew, T. L.; Bulović, V.; Swager, T. M. Improving the Performance of P3HT-Fullerene Solar Cells with Side-Chain-Functionalized Poly(thiophene) Additives: A New Paradigm for Polymer Design. *ACS Nano* **2012**, *6*, 3044−3056.

(18) Liao, H. C.; Ho, C. C.; Chang, C. Y.; Jao, M. H.; Darling, S. B.; Su, W. F. Additives for Morphology Control in High-Efficiency Organic Solar Cells. *Mater. Today* **2013**, *16*, 326−336.

(19) Liao, H. C.; Tsao, C. S.; Shao, Y. T.; Chang, S. Y.; Huang, Y. C.; Chuang, C. M.; Lin, T. H.; Chen, C. Y.; Su, C. J.; Jeng, U. S.; Chen, Y. F.; Su, W. F. Bi-hierarchical Nanostructures of Donor-Acceptor Copolymer and Fullerene for High Efficient Bulk Heterojunction Solar Cells. *Energy Environ. Sci.* **2013**, *6*, 1938−1948.

(20) Chang, S. Y.; Liao, H. C.; Shao, Y. T.; Sung, Y. M.; Hsu, S. H.; Ho, C. C.; Su, W. F.; Chen, Y. F. Enhancing the Efficiency of Low Bandgap Conducting Polymer Bulk Heterojunction Solar Cells Using P3HT as A Morphology Control Agent. *J. Mater. Chem. A* **2013**, *1*, 2447−2452.

(21) Shankar, K.; Feng, X.; Grimes, C. A. Enhanced Harvesting of Red Photons in Nanowire Solar Cells: Evidence of Resonance Energy Transfer. *ACS Nano* **2009**, *3*, 788−794.

(22) Andrews, D. L.; Curutchet, C.; Scholes, G. D. Resonance Energy Transfer: Beyond the Limits. *Laser Photonics Rev.* **2011**, *5*, 114−123.

(23) Sun, B.; Zhang, Y.; Gu, K. J.; Shen, Q. D.; Yang, Y.; Song, H. Layer-by-Layer Assembly of Conjugated Polyelectrolytes on Magnetic Nanoparticle Surfaces. *Langmuir* **2009**, *25*, 5969−5973.

(24) Chen, M. C.; Liaw, D. J.; Chen, W. H.; Huang, Y. C.; Sharma, J.; Tai, Y. Improving the Efficiency of an Organic Solar Cell by a Polymer Additive to Optimize the Charge Carriers Mobility. *Appl. Phys. Lett.* **2011**, *99*, 223305.

(25) Lian, W. R.; Huang, Y. C.; Liao, Y. A.; Wang, K. L.; Li, L. J.; Su, C. Y.; Liaw, D. J.; Lee, K. R.; Lai, J. Y. Flexible Electrochromic Devices Based on Optoelectronically Active Polynorbornene Layer and Ultratransparent Graphene Electrodes. *Macromolecules* **2011**, *44*, 9550−9555.

(26) Lee, E.; Kim, C.; Jang, J. High-Performance Förster Resonance Energy Transfer (FRET)-Based Dye-Sensitized Solar Cells: Rational Design of Quantum Dots for Wide Solar-Spectrum Utilization. *Chem.—Eur. J.* **2013**, *19*, 10280−10286.

(27) Reil, F.; Hohenester, U.; Krenn, J. R.; Leitner, A. Förster-type Resonant Energy Transfer Influenced by Metal Nanoparticles. *Nano Lett.* **2008**, *8*, 4128−4133.

(28) Grimes, A. F.; Call, S. E.; Harbron, E. J.; English, D. S. Wavelength-Resolved Studies of Förster Energy Transfer in Azobenzene-Modified Conjugated Polymers: The Competing Roles

of Exciton Migration and Spectral Resonance. *J. Phys. Chem. C* **2007**, *111*, 14257−14265.
(29) Feron, K.; Belcher, W. J.; Fell, C. J.; Dastoor, P. C. Organic Solar Cells: Understanding the Role of Förster Resonance Energy Transfer. *J. Mol. Sci.* **2012**, *13*, 17019−17047.
(30) Guillain, F.; Tsikritzis, D.; Skoulatakis, G.; Kennou, S.; Wantz, G.; Vignau, L. Annealing-Free Solution-Processed Tungsten Oxide for Inverted Organic Solar Cells. *Sol. Energy Mater. Sol. Cells* **2014**, *122*, 251−256.
(31) Choi, K. C.; Lee, E. J.; Baek, Y. K.; Kim, M. J.; Kim, Y. D.; Shin, P. W.; Kim, Y. K. Modifying Hydrogen Bonding Interaction in Solvent and Dispersion of ZnO Nanoparticles: Impact on the Photovoltaic Performance of Inverted Organic Solar Cells. *RSC Adv.* **2014**, *4*, 7160−7166.
(32) Ho, C. R.; Tsai, M. L.; Jhuo, H. J.; Lien, D. H.; Lin, C. A.; Tsai, S. H.; Wei, T. C.; Huang, K. P.; Chen, S. A.; He, J. H. An Energy-Harvesting Scheme Employing $CuGaSe_2$ Quantum Dot-Modified ZnO Buffer Layers for Drastic Conversion Efficiency Enhancement in Inorganic-Organic Hybrid Solar Cells. *Nanoscale* **2013**, *5*, 6350−6355.
(33) Mizukami, S.; Hori, Y.; Kikuchi, K. Small-Molecule-Based Protein-Labeling Technology in Live Cell Studies: Probe-Design Concepts and Applications. *Acc. Chem. Res.* **2014**, *47*, 247−256.
(34) Kumar, P.; Pal, S. K. Role of Decoupled Defect Transitions of ZnO Nanocrystals in Energy Transfer. *J. Photochem. Photobiol., A* **2014**, *278*, 46−52.
(35) Huang, J. S.; Goh, T.; Li, X.; Sfeir, M. Y.; Bielinski, E. A.; Tomasulo, S.; Lee, M. L.; Hazari, N.; Taylor, A. D. Polymer Bulk Heterojunction Solar Cells Employing Förster Resonance Energy Transfer. *Nat. Photonics* **2013**, *7*, 479−485.
(36) Koppe, M.; Egelhaaf, H. J.; Dennler, G.; Scharber, M. C.; Brabec, C. J.; Schilinsky, P.; Hoth, C. N. Near IR Sensitization of Organic Bulk Heterojunction Solar Cells: Towards Optimization of the Spectral Response of Organic Solar Cells. *Adv. Funct. Mater.* **2010**, *20*, 338−346.
(37) Ameri, T.; Min, J.; Li, N.; Machui, F.; Baran, D.; Forster, M.; Schottler, K. J.; Dolfen, D.; Scherf, U.; Brabec, C. J. Performance Enhancement of the P3HT/PCBM Solar Cells through NIR Sensitization Using a Small-Bandgap Polymer. *Adv. Energy Mater.* **2012**, *2*, 1198−1202.
(38) Huang, Y. C.; Chia, H. C.; Chuang, C. M.; Tsao, C. S.; Chen, C. Y.; Su, W. F. Facile Hot Solvent Vapor Annealing for High Performance Polymer Solar Cell Using Spray Process. *Sol. Energy Mater. Sol. Cells* **2013**, *114*, 24−30.
(39) Huang, J. H.; Ho, Z. Y.; Kekuda, D.; Chang, Y.; Chu, C. W.; Ho, K. C. Effects of Nanomorphological Changes on the Performance of Solar Cells with Blends of Poly[9,9′-dioctyl-fluorene-co-bithiophene] and a Soluble Fullerene. *Nanotechnology* **2009**, *20* (2), 025202.
(40) Murgatroyd, P. N. Theory of Space-Charge-Limited Current Enhanced by Frenkel Effect. *J. Phys. D: Appl. Phys.* **1970**, *3*, 151−156.
(41) Xin, H.; Guo, X.; Kim, F. S.; Ren, G.; Watson, M. D.; Jenekhe, S. A. Efficient Solar Cells Based on a New Phthalimide-Based Donor-Acceptor Copolymer Semiconductor: Morphology, Charge-Transport, and Photovoltaic Properties. *J. Mater. Chem.* **2009**, *19*, 5303−5310.
(42) Lin, J. F.; Tu, G. Y.; Ho, C. C.; Chang, C. Y.; Yen, W. C.; Hsu, S. H.; Chen, Y. F.; Su, W. F. Molecular Structure Effect of Pyridine-Based Surface Ligand on the Performance of P3HT:TiO_2 Hybrid Solar Cell. *ACS Appl. Mater. Interfaces* **2013**, *5*, 1009−1016.
(43) Goffri, S.; Müller, C.; Stingelin-Stutzmann, N.; Breiby, D. W.; Radano, C. P.; Andreasen, J. W.; Thompson, R.; Janssen, R. A. J.; Nielsen, M. M.; Smith, P.; Sirringhaus, H. Multicomponent Semiconducting Polymer Systems with Low Crystallization-Induced Percolation Threshold. *Nat. Mater.* **2006**, *5*, 950−956.
(44) Ma, W.; Zhang, J.; Wang, X.; Wang, S. Effect of PMMA on Crystallization Behavior and Hydrophilicity of Poly(vinylidene fluoride)/Poly(methyl methacrylate) Blend Prepared in Semi-dilute Solutions. *Appl. Surf. Sci.* **2007**, *253*, 8377−8388.
(45) Peesan, M.; Supaphol, P.; Rujiravanit, R. Preparation and Characterization of Hexanoyl Chitosan/Polylactide Blend Films. *Carbohydr. Polym.* **2005**, *60*, 343−350.